Results of the Department of Space Physics, Institute of Atmospheric Physics, Czech Academy of Sciences, published in 2024

1. Strong effects of chorus waves on radiation belts expected for future magnetic superstorms

We employ extensive databases of spacecraft observations to determine how lower-band whistler mode chorus waves behave under extreme geomagnetic conditions. Chorus occurring close to the geomagnetic equator is known for causing rapid increases of ultra-relativistic electron fluxes under disturbed geomagnetic conditions. However, chorus can also propagate to high latitudes and here its presence may lead to losses of these electrons. We showed that under extreme geomagnetic conditions, amplitudes of chorus waves at high latitudes grow much slower than chorus amplitudes close to the equator. They therefore have a net effect of accelerating ultra-relativistic electrons, which results in an increase of fluxes at multi-MeV energies by several orders of magnitude.

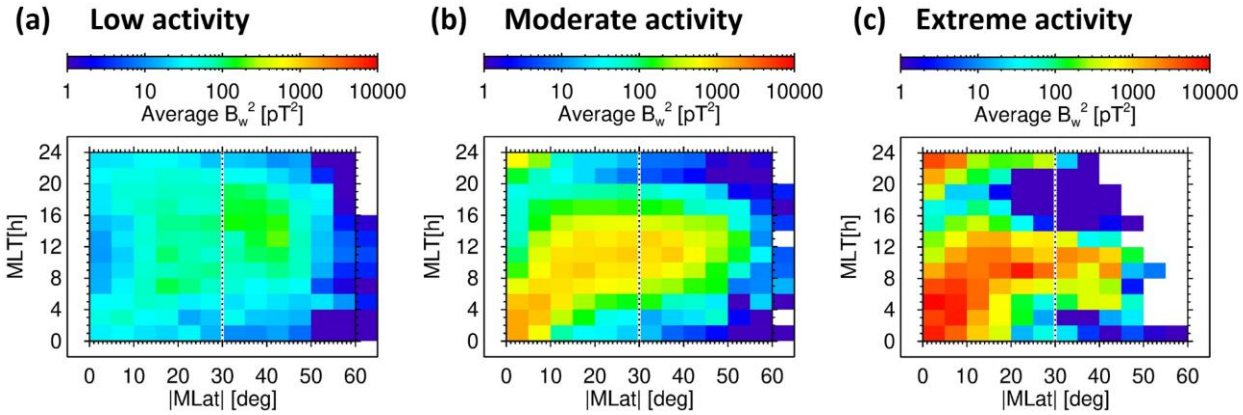

External driving of chorus. *Color scale shows the long-term average squared amplitudes of chorus magnetic field fluctuations in pT^2. A joint data set of two Van Allen Probes and four Cluster spacecraft is analyzed in 12x13 discrete bins in magnetic local time and absolute value of magnetic latitude, where cumulative results for latitudes above 60° are shown on the outer edge of the plot. (A) Data from periods of low geomagnetic activity: see Supplementary Method 4; (B) the same for moderate geomagnetic activity; (C) the same for extreme cases of the highest geomagnetic activity. A vertical dotted line shows an approximate boundary between the equatorial region, where chorus strongly responds to geomagnetic activity, and the high-latitude region, where the response is weak.*

Reference:

Santolík, O., Shprits, Y., **Kolmašová, I.**, Wang, D., **Taubenschuss, U.**, **Turčičová, M.**, & **Hanzelka, M.** (2024). Strong effects of chorus waves on radiation belts expected for future magnetic superstorms. *AGU Advances, 5*, e2024AV001234. Doi.10.1029/2024AV001234.

Related references:

Němec, F., **Santolík, O**., Hospodarsky, G. B., & Kurth, W. S. (2024). Magnetospheric line radiation: Temporal modulation corresponding to a bouncing wave. *Geophysical Research Letters, 51*, e2024GL111477. Doi: 10.1029/2024GL111477.

Němec, F., **Santolík, O.**, Hospodarsky, G. B., & Kurth, W. S. (2024). Quasiperiodic emissions: Fine structure corresponding to a bouncing wave. *Geophysical Research Letters, 51*, e2023GL106459. Doi:10.1029/2023GL106459.

Shen, X., Li, W., Ma, Q., Qin, M., Capannolo, L., Gan, L., **Hanzelka, M.**, Sheng, H., Chu, X. (2024), Large Amplitude Whistler Waves in Earth's Plasmasphere and Plasmaspheric Plumes, *Geophysical Research Letters, 51*, e2023GL105244. Doi: 10.1029/2023GL105244.

Grimmich, N., Plaschke, F., **Grison, B.**, Prencipe, F., Escoubet, C. P., Archer, M. O., Constantinescu, O. D., Haaland, S., Nakamura, R., Sibeck, D. G., Darrouzet, F., Hayosh, M., and Maggiolo, R. (2024), The Cluster spacecrafts' view of the motion of the high-latitude magnetopause, Ann. Geophys., 42, 371–394. Doi:10.5194/angeo-42-371-2024.

Jung, J., Connor, H. K., Dimmock, A.P., Sembay, S., Read, A. M., **Souček, J.** (2024), Mshpy23: a user-friendly, parameterized model of magnetosheath conditions, *Earth and Planetary Physics*, 8, 1, 89-104. Doi: 10.26464/epp2023065.

2. Whistler echo trains triggered by energetic winter lightning

Lightning generated electromagnetic impulses propagating in the magnetospheric plasma disperse into whistlers – several seconds long radio wave signals with decreasing frequency. Sometimes, multiple reflections form long echo trains containing many whistlers with increasing dispersion. On January 3, 2017, two necessary prerequisites – a pronounced lightning activity and a magnetospheric plasma duct – allowed for observations of a large number of whistler echo trains by the high-latitude station in Kannuslehto, Finland. Our investigation reveals that the duct existed for nearly eight hours. We show that causative lightning sferics arrived to the duct entry from three different winter thunderstorms: a small storm at the Norwegian coast, which produced energetic lightning capable to trigger echo trains in 50% of cases, and two large storms at unexpectedly distant locations in the Mediterranean region. Our results show that intense thunderstorms can repetitively feed electromagnetic energy into a magnetospheric duct and form whistler echo trains after subionospheric propagation over distances as large as 4000 km.

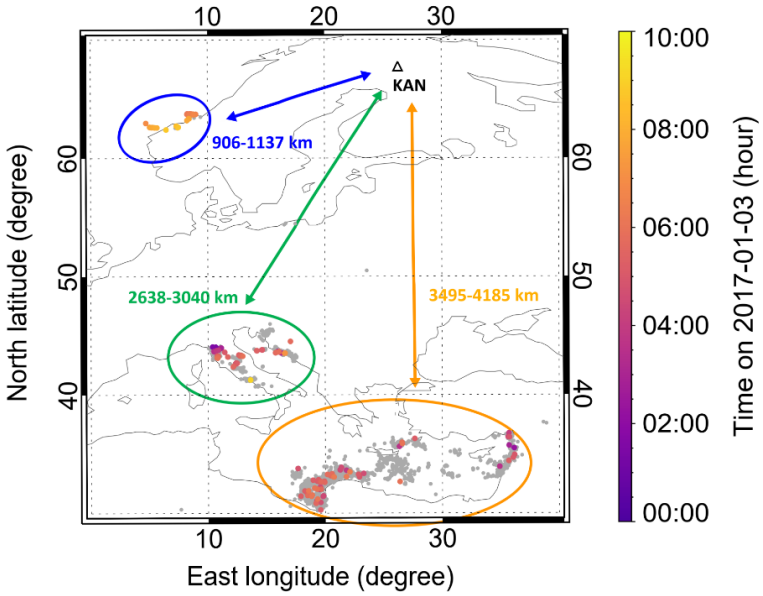

The locations of lightning discharges from the consolidated list of EUCLID and WWLLN detections (in grey) are shown, with the source lightning discharges for echo trains in color coded by the time of their occurrence. The colors correspond to the time of lightning occurrence. The colored ovals mark three separated areas with the lightning activity (Northern thunderstorm – blue, Central Mediterranean – green, and Eastern and African Mediterranean – orange).

Reference:

Kolmašová, I., **Santolík**, O. & Manninen, J. (2024), Whistler echo trains triggered by energetic winter lightning. *Nature Communications 15*, 7166. Doi:10.1038/s41467-024-51684-0.

Related references:

Linzmayer, V., Němec, F., **Santolík, O.**, & **Kolmašová, I.** (2024). Lightning-induced energetic electron precipitation observed in long-term DEMETER spacecraft measurements. *Journal of Geophysical Research: Space Physics, 129*, e2024JA032713. Doi:10.1029/2024JA032713.

3. Sub-MeV Electron Precipitation Driven by EMIC Waves through Nonlinear Fractional Resonances

Electromagnetic ion cyclotron waves in the Earth's outer radiation belt drive rapid electron losses through wave-particle interactions. The precipitating electron flux can be high in the hundreds of keV energy range, well below the typical minimum resonance energy. One of the proposed explanations relies on nonresonant scattering, which causes pitch-angle diffusion away from the fundamental cyclotron resonance. Here we propose the fractional sub-cyclotron resonance, a second-order nonlinear effect that scatters particles at resonance order n = 1/2, as an alternate explanation. Using test-particle simulations, we evaluate the precipitation ratios of sub-MeV electrons for wave packets with various shapes, amplitudes, and wave normal angles. We show that the nonlinear sub-cyclotron scattering produces larger ratios than the nonresonant scattering when the wave amplitude reaches sufficiently large values.

The ELFIN CubeSats detected several events with precipitation ratio patterns matching our simulation, demonstrating the importance of sub-cyclotron resonances during intense precipitation events.

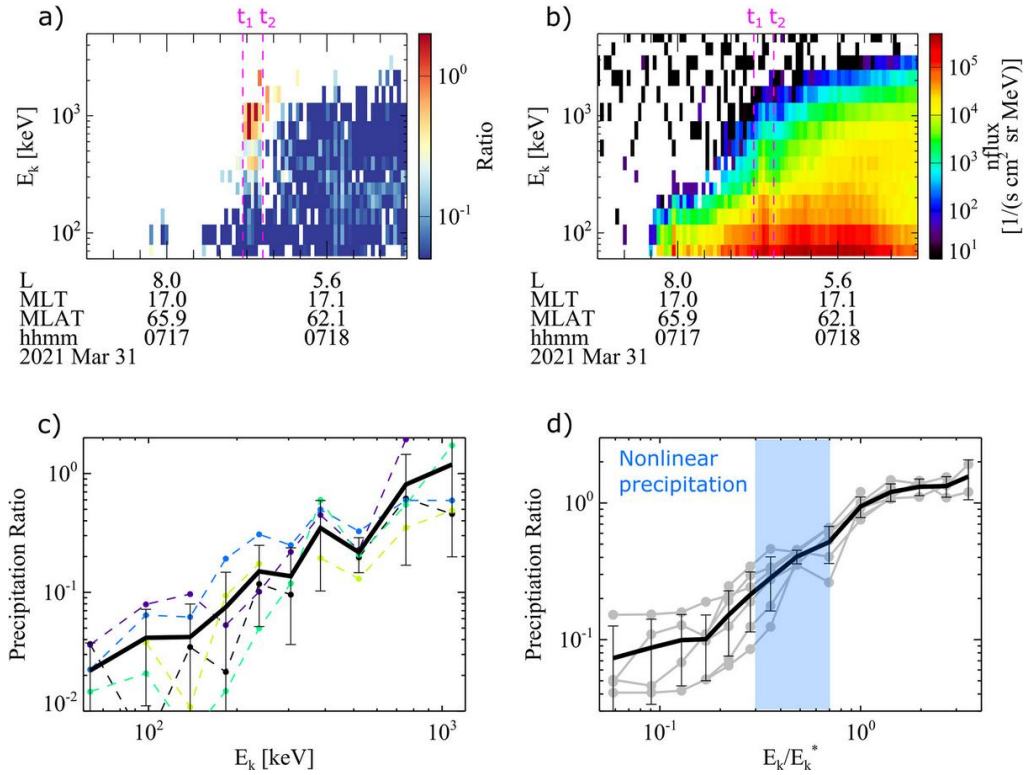

Electron precipitation detected by the ELFIN CubeSats. (a) Precipitation ratios detected by ELFIN-A on 31 March 2021 in the northern hemisphere, with a typical EMIC-driven precipitation pattern shown between t_1 = 07:17:30 and t_2 = 07:17:33 (dashed magenta lines). (b) Trapped electron number flux. (c) Line plots of precipitation ratios between t_1 and t_2, with each dashed colored line representing a single half-spin and the thick black line showing the average with standard deviations as error bars. (d) Statistical precipitation ratios in selected events plotted against normalized energy. Gray lines represent averages over individual events; the black line is the sample average with error bars showing the standard deviations. The light blue area highlights the energy range where the strongest effects from the n = 1/2 nonlinear resonance are expected.

Reference:

Hanzelka, M., Li, W., Qin, M.,Capannolo, L., Shen, X., Ma, Q., Gan, L., & Angelopoulos, V. (2024), Sub-MeV Electron Precipitation Driven by EMIC Waves through Nonlinear Fractional Resonances, *Geophysical Research Letters, 51*, e2023GL107355. Doi: 10.1029/2023GL107355.

Related reference:

Haas, B., Shprits, Y., Himmelsbach, J., Wang, D., Drozdov, A., Szabo-Roberts, M. & **Hanzelka, M**. (2024), Modeling pitch angle dependent electron precipitation using electron lifetimes*, Journal of Geophysical Research: Space Physics, 129(10),* e2024JA032554. Doi: 10.1029/2024JA032554.

4. Electromagnetic model of K-changes

Electromagnetic Model of K-Changes K-changes are observed as step-like increases in the thundercloud electric fields. The K-changes occur in the late part of intra-cloud lightning or during negative cloud-to-ground lightning between return strokes. We introduce a new model to simulate processes leading to the K-changes in cloud-to-ground lightning. Our method is based on the full solution of Maxwell's equations coupled to Poisson's equation for the thundercloud charge structure. To model the K-changes, we gradually increase the decayed channel conductivity. The modeled current wavefront propagates due to the K-processes downward along a vertical channel and completely attenuates before reaching the ground. We derive the evolution of the linear chargé densities and the scalar electric potential along the channel leading to K-changes. We model electrostatic step like changes in the measured electric field together with the approximate rates and amplitudes of the microsecond scale pulses. Step-like changes increase their amplitudes with the length of the simulated channel and with a higher conductivity of the channel. The microsecond-scale pulse wave shapes depend mainly on the propagation velocity of the current wave, and the time scale of the conductivity increase. We show that our modeled waveforms are in a good agreement with observations conducted in Florida.

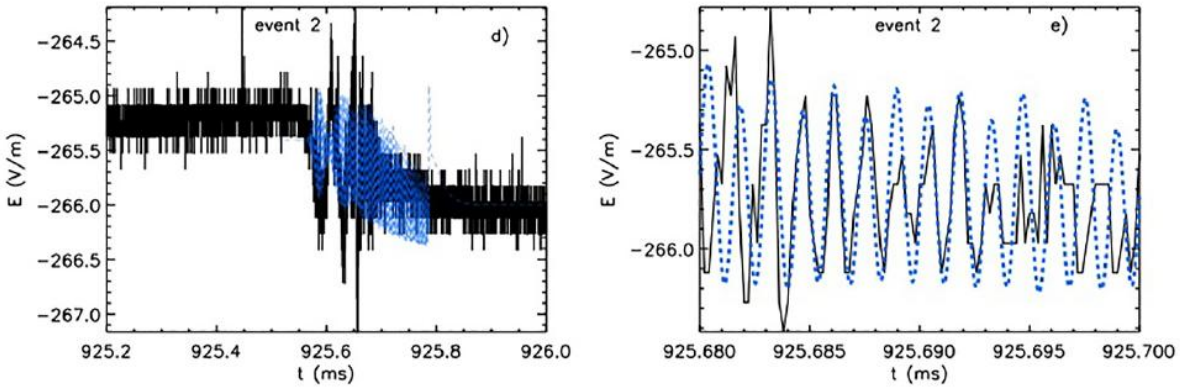

Measured electric field data (black line) together with the modeled waveforms (blue line) and the enlarged part of the electric field waveforms.

Reference:

Kašpar, P., Marshall, T., Stolzenburg, M., **Kolmašova, I.,** & **Santolik, O.** (2024). Electromagnetic model of K-changes. *Journal of Geophysical Research: Atmospheres*, 129, e2023JD040503. Doi.10.1029/2023JD040503.

Related reference:

Chum, J., Langer, R., **Kolmašová, I.**, Lhotka, O., Rusz, J., Strhárský, I. (2024), Solar cycle signatures in lightning activity, *Atmospheric Chemistry and Physics*, 24, 16, 9119-9130. Doi:10.5194/acp-24-9119-2024.

5. Ray-tracing analysis for the propagation of Saturn narrowband emission within the Saturnian magnetosphere

This study investigates the propagation characteristics of Saturn's Narrowband (NB) emissions using a 3D ray-tracing code incorporating Saturn's magnetic field and electron density parameters. The potential source regions and propagation zones of the L-O mode, Z mode and whistler mode NB emissions are distinguished. The L-O mode NB emissions, generated along local electron plasma frequency surfaces through mode conversion, exhibit straight-line propagation but undergo reflections between the ionosphere, the plasma torus, and the magnetosheath. The slot region, characterized by a lower electron density distributed around the plasma torus boundary, significantly influences emission propagation, potentially leading to trapping and depolarization. The 5 kHz Z mode NB emissions propagate and fill the trapping region delineated by lower cutoff and upper hybrid resonance frequencies. In contrast, the 20 kHz Z mode NB emissions are primarily confined near source regions at the north and south edges of the plasma torus, with the possibility of escaping under variable plasma conditions.

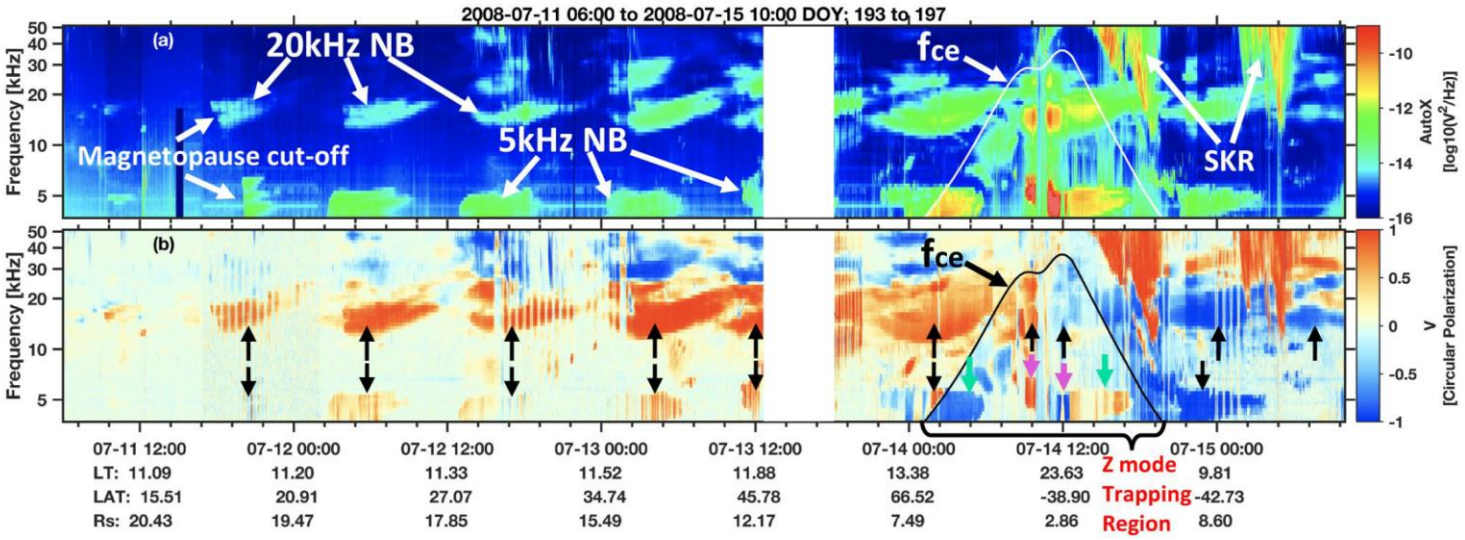

Observation examples of Saturn Narrowband emissions during an interval from 2008-07-11 6:00 to 2008-07-15 10:00. Panels (a)–(b) present the spectrogram of the Cassini Radio and Plasma Wave Science (RPWS) electric field intensity, as well as the circular. The arrows in Panel (b) indicate the different modes of NB emissions: black for L-O mode, green for ZR-X mode, and pink for ZL-X mode. The white and black curves in Panels (a)–(b) represent the local electron cyclotron frequency f_{ce}. The intensity modulation of the spectrogram (vertical stripes) near 07-11 22:00 and 07-12 18:00 is due to the rolling of Cassini spacecraft.

Reference:

Wu, S., **U. Taubenschuss**, S.-Y. Ye, G. Fischer, B. Cecconi, M. Wang, T. Tao, M. Long, P. Lu, Y. Liu, W. S. Kurth, C. M. Jackman, P. Zarka, C. Baskevitch, & X. Feng (2024), Ray-tracing analysis for the propagation of Saturn narrowband emission within the Saturnian magnetosphere, *Journal of Geophysical Research: Planets,* 129, 4. Doi:10.1029/2023JE008118.

Related references:

Wu, S., S.-Y. Ye, **U. Taubenschuss**, G. Fischer, C. M. Jackman, P. Zarka, W. S. Kurth, M. Wang, B. Cecconi, H. Ning, M. Long, & C. Baskevitch (2024), Formation of an extended equatorial shadow zone for low-frequency Saturn kilometric radiation, *Geophysical Research Letters, 51*, 15. Doi:10.1029/2023GL106652.

Boudouma, A., P. Zarka, C. K. Louis, C. Briand, and **M. Imai** (2024), Generation mechanism and beaming of Jovian nKOM from 3D numerical modeling of Juno/Waves observations, *Journal of Geophysical Research: Space Physics*, 129, e2023JA032280. Doi:10.1029/2023JA032280.

6. Radial Variations in Solar Type III Radio Bursts

Type III radio bursts are generated by electron beams accelerated at reconnection sites in the corona. This study, utilizing data from the Parker Solar Probe's first 17 encounters, closely examines these bursts down to 13 solar radii. A focal point of our analysis is the near-radial alignment (within 5°) of the Parker Solar Probe, STEREO-A, and Wind spacecraft relative to the Sun. This alignment, facilitating simultaneous observations of 52 and 27 bursts by STEREO-A and Wind respectively, allows for a detailed differentiation of radial and longitudinal burst variations. Our observations reveal no significant radial variations in electron beam speeds, radio fluxes, or exponential decay times for events below 50 solar radii. In contrast, closer to the Sun we noted a decrease in beam speeds and radio fluxes. This suggests potential effects of radio beaming or alterations in radio source sizes in this region. Importantly, our results underscore the necessity of considering spacecraft distance in multispacecraft observations for accurate radio burst analysis. A critical threshold of 50 solar radii emerges, beyond which beaming effects and changes in beam speeds and radio fluxes become significant. Furthermore, the consistent decay times across varying radial distances point toward a stable trend extending from 13 solar radii into the inner heliosphere. Our statistical results provide valuable insights into the propagation mechanisms of type III radio bursts, particularly highlighting the role of scattering near the radio source when the frequency aligns with the local electron plasma frequency.

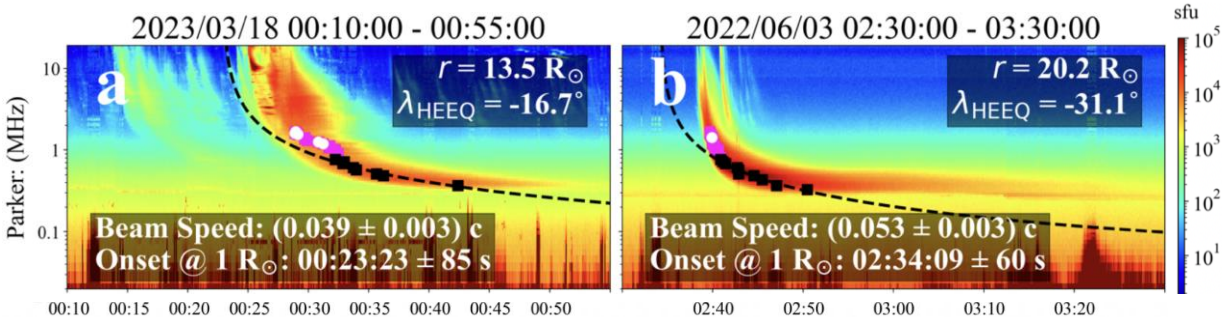

Radio measurements from the Parker Solar Probe (panels (a)–(b) on 2023 March 18 between 00:10 and 00:55 UT (Case #1, left), on 2022 June 3 between 02:30 and 03:30 UT. Panels mark peak fluxes within our targeted frequency range using squares. Black squares denote peak fluxes used to calculate electron beam speeds based on the empirical density model, with fitted electron beams shown by black dashed lines and the computed speeds and onset times at 1 Rs noted in each panel. Magenta squares highlight peak fluxes outside our propagation analysis frequency range. White circles indicate peak fluxes when the wave vector

azimuth was within 5°, implying minimal radio propagation variation and suggesting that the type III bursts originated near the line connecting the Parker Solar Probe and the Sun.

Reference:

Krupar, V., Kruparova, O., Szabo, A., Wilson, L. B., Nemec, F., **Santolik, O**., Pulupa, M., Issautier, K., Bale, S. D., & Maksimovic, M. (2024), Radial Variations in Solar Type III Radio Bursts, *Astrophys. J. Lett.*, 967 (2): Art. No. L32. Doi:10.3847/2041-8213/ad4be7.

Related references:

Kociscak, S., Kvammen, A., Mann, I., Meyer-Vernet, N., **Píša, D.**, **Souček, J.**, Theodorsen, A., Vaverka, J., Zaslavsky, A. (2024), Impact ionization double peaks analyzed in high temporal resolution on Solar Orbiter, *Annales Geophysicae*, 42, 1, 191-212. Doi: 10.5194/angeo-42-191-202.

Boldú, J. J., Graham, D. B., Morooka, M., André, M., Khotyaintsev, Y. V., Dimmock, A., **Píša, D.**, **Souček, J.** et al., 2024: Ion-Acoustic Waves Associated With Interplanetary Shocks, *Geophysical Research Letters*, 51, 16, e2024GL109956. Doi: 10.1029/2024GL109956.

Edberg, N.J.T., Andrews, D.J., Boldú, J.J., (...), **Píša, D**. et al. (2024), Extent of the Magnetotail of Venus From the Solar Orbiter, Parker Solar Probe and BepiColombo Flybys, *Journal of Geophysical Research: Space Physics*, 129, 10, e2024JA032603. Doi: 0.1029/2024JA032603.

R. Kieokaew, R.F. Pinto, E. Samara, C. Tao, M. Indurain, B. Lavraud, A. Brunet, V. Génot, A. Rouillard, N. André, S. Bourdarie, C. Katsavrias, F. Darrouzet, **B. Grison**, I. Daglis (2024), Helio1D modeling of temporal variation of solar wind: Interfacing between MULTI-VP and 1D MHD for future operational forecasting at L1, *J. Space Weather Space Clim.* 14 19. Doi:10.1051/swsc/2024018.

T. Baratashvili, **B. Grison**, B. Schmieder, P. Démoulin and S. Poedts (2024), Multi-spacecraft study with the Icarus model - Modelling the propagation of CMEs to Mercury and Earth, *A&A*, 689 A98. Doi:10.1051/0004-6361/20245043.

7. The Comet Interceptor mission

We describe the novel, multi-point Comet Interceptor mission. It is dedicated to the exploration of a little-processed long-period comet, possibly entering the inner Solar System for the first time, or to encounter an interstellar object originating at another star. The objectives of the mission are to address the following questions: What are the surface composition, shape, morphology, and structure of the target object? What is the composition of the gas and dust in the coma, its connection to the nucleus, and the nature of its interaction with the solar wind? The mission was proposed to the European Space Agency in 2018, and formally adopted by the agency in June 2022, for launch in 2029 together with the Ariel mission. Comet Interceptor will take advantage of the opportunity presented by ESA's FClass call for fast, flexible, low-cost missions to which it was proposed. The call required a launch to a halo orbit around the Sun-Earth L2 point. The mission can take advantage of this placement to wait for the discovery of a suitable comet reachable with its minimum ΔV capability of 600 ms−1. Comet Interceptor will be unique in encountering

and studying, at a nominal closest approach distance of 1000 km, a comet that represents a near-pristine sample of material from the formation of the Solar System. It will also add a capability that no previous cometary mission has had, which is to deploy two sub-probes – B1, provided by the Japanese space agency, JAXA, and B2 – that will follow different trajectories through the coma. While the main probe passes at a nominal 1000 km distance, probes B1 and B2 will follow different chords through the coma at distances of 850 km and 400 km, respectively. The result will be unique, simultaneous, spatially resolved information of the 3-dimensional properties of the target comet and its interaction with the space environment. We present the mission's science background leading to these objectives, as well as an overview of the scientific instruments, mission design, and schedule.

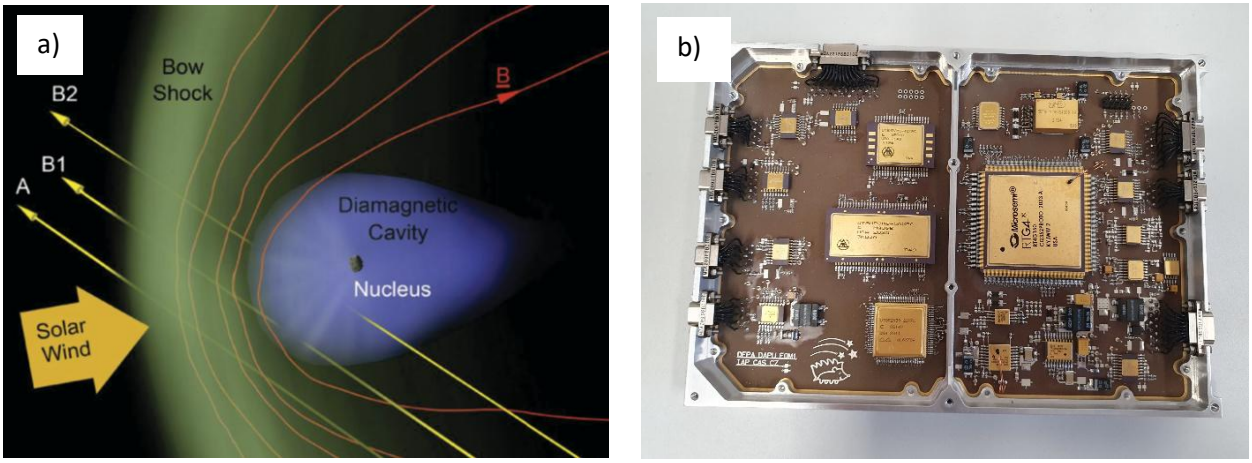

a) Multi-point measurements will determine the scale and shape of several structures in the comet-solar wind interaction. The time at which each of the three spacecraft/probes cross (or do not cross) the bow shock (green) and diamagnetic cavity (blue) will determine their shapes and scales. The magnetic field (red) will also be probed using magnetometers on all the three platforms. b) Electronic board of the engineering model of the DAPU (Dust Analyzer & Processing Unit) instrument developed at the Department of Space Physics for the probe A.

Reference:

Jones, G. H., Snodgrass, C., Tubiana, C., (...), **Kolmašová, I., Grison, B., Jánský, J**., Kohout, T., **Lán, R., Santolík, O., Souček, J., Uhlíř, L.** et al. (2024), The Comet Interceptor Mission, *Space Science Reviews*, 220, 1, 9. Doi: 10.1007/s11214-023-01035-0.

Related reference:

De Keyser, J., Edberg, N.J.T., Henri, P., Auster, H.-U., Galand, M., Rubin, M., Nilsson, H., **Souček, J**. et al. (2024), In situ plasma and neutral gas observation time windows during a comet flyby: Application to the Comet Interceptor mission, *Planetary and Space Science*, 244, 105878. Doi:10.1016/j.pss.2024.105878.

8. Hands-on Manufacturing Education: Radio Reception Experiment from KOSEN CubeSat Using Cardboard Yagi Antenna

Recently, utilizing a small satellite, such as CubeSat, for space education has gained global attention. The KOSEN-1 CubeSat, developed by National Institute of Technology (abbreviated as KOSEN in Japanese), has been transmitting continuous waves while in orbit around Earth since 2021. Building a cheap and reliable antenna to receive these waves from the amateur satellites like KOSEN-1 is a significant matter. In 2023, we conducted hands-on manufacturing workshops four times to build cardboard Yagi antennas for KOSEN students and the general public. Each workshop included the steps of building the antenna by hand and using it to receive radio waves from KOSEN-1. In this paper, we report a summary of these workshops and evaluate the results of the questionnaires filled out by the participants.

Reference:

Imai, M., K. Imai, M. Tsuji, M. Tokumitsu, and M. Wakabayashi (2024), Hands-on Manufacturing Education: Radio Reception Experiment from KOSEN CubeSat Using Cardboard Yagi Antenna (in Japanese), *J. JSEE*, 72(5), 5_117-5_122. Doi:10.4307/jsee.72.5_117.

Department of Space Physics, Institute of Atmospheric Physics of the Czech Academy of Sciences in 2024

1. Radka Balková, secretary, 50% FTE
2. Tomáš Formánek, student, 20% FTE, *from 1 September 2024 on leave in Observatoire de Paris*
3. Benjamin Grison, research scientist
4. Michajlo Hajoš, research scientist
5. *Miroslav Hanzelka, postdoctoral associate, on leave at GFZ Potsdam*
6. Pavel Houfek, research engineer, from 1 October 2024 also PhD student
7. Masafumi Imai, research scientist, from 1 April 2024
8. Jiří Jánský, research engineer
9. *Michaela Jírová, PhD student, on parental leave*
10. Petr Kašpar, research scientist
11. Vavřinec Kavan, student, 20% FTE
12. Andrea Kolínská, PhD student, 70% FTE
13. Ivana Kolmašová, senior research scientist
14. *Vratislav Krupař, research scientist, on leave in NASA GSFC*
15. *Oksana Krupařová, research scientist, on leave in NASA GSFC*
16. Radek Lán, research engineer
17. Ján Mičko, PhD student, 70% FTE
18. David Píša, research scientist
19. Martin Popek, TLE observer, 25% FTE
20. Kateřina Rosická, student, 20% FTE, from 1 October 2024 PhD student, 70% FTE
21. Ondřej Santolík, senior research scientist, head of the department
22. Jan Snížek, research engineer, 50% FTE
23. Jan Souček, senior research scientist, deputy head of the department
24. *Hana Špačková, PhD student, on parental leave*
25. Ulrich Taubenschuss, research scientist
26. Luděk Uhlíř, research engineer
27. Jaroslav Vojta, research engineer, 10% FTE